Journal of Structural Geology, Vol. 14, No. 6, pp. 689 to 699, 1992
Printed in Great Britain

0191-8141/92 $05.00+0.00

Geometry and kinematics of active faults and their seismotectonic significance in the western Corinth–Patras rift (Greece)

THEODOR DOUTSOS and GEORGIOS POULIMENOS

Department of Geology, University of Patras, Patras 26110, Greece.

(*Received* 26 *March* 1991; *accepted in revised form* 4 *January* 1992)

Abstract—The western part of the Corinth–Patras rift is formed in an area which is being uplifted. Rifted domains have subsided relative to the adjacent areas in NW Peloponnesus and Sterea Hellas, but subsidence rates rarely exceed uplift rates. Extension is mainly accomplished by WNW-trending active faults with lengths up to 25 km. Most of these faults show an along-strike segmentation and often terminate against transfer faults.

Displacement analysis, along 170 mesoscopic faults and 36 mappable faults, has been carried out to assess slip rates and to estimate the magnitudes and recurrence time intervals of earthquakes occurring along them. Earthquake magnitude ranges between 5 and 6.7. Only eight faults appear to be capable of producing earthquake magnitudes larger than 6. Recurrence times of these large earthquakes vary between 80 and 1690 years.

Upper crustal deformation in the western Corinth graben can be described by six large asymmetric grabens which are inferred to bottom out to a N-dipping curved ramp. The asymmetric shape of most WNW-trending rifts in the Hellenic peninsula, including the Corinth–Patras rift promotes the simple shear model of extension against the pure shear model in the upper crustal layer.

INTRODUCTION

THE Aegean area is one of the most rapidly extending continental areas in the world (McKenzie 1978, Angelier 1979, Jackson & McKenzie 1988). In the Hellenic peninsula Quaternary extension is reflected by WNW-trending rift belts, spaced typically ~40 km apart (Fig. 1a). Most of this extension is taken up on major normal faults which reach a depth of about 8–12 km, as revealed by large earthquakes occurring at Thessaloniki, Kalamata and Alkyonides (in the eastern gulf of Corinth) (Papazachos *et al.* 1979, Jackson *et al.* 1982, Lyon *et al.* 1988). Although, there is some published field work concerning the orientation and kinematics of the faults (Mercier 1977, Sebrier 1977, Doutsos 1980, Pavlides & Mountrakis 1987, Zelilidis *et al.* 1988), and their shape and linkage (Dewey & Şengör 1979, Brooks *et al.* 1988, Doutsos *et al.* 1988), the movements along normal faults have not been quantitatively analysed and compared with the characteristics of earthquakes. To this purpose we chose one of the most seismically active areas of the Aegean region: the western part of the Corinth–Patras rift in NW Peloponnesus (Fig. 1b). As studies of micro-earthquake distribution in that area are available (Fig. 1c) (Drakopoulos *et al.* 1987, Melis *et al.* 1989), we have compared these with our neotectonic data to arrive at an overall picture of crustal movements.

TECTONIC SETTING

Field work was carried out in a 5000 km^2 area in the NW Peloponnesus (Fig. 2a), the central part of which extends above the crustal root zone of West Hellenides. Extensive geological research (Philippson 1892, Aubouin 1959, Dercourt 1964, Jacobshagen *et al.* 1978) has revealed a W-verging stack of flat-lying nappes (Fig. 1a). The Plattenkalk nappe at the base, the Phyllites and the Gavrovo–Tripolitsa nappe in the middle and the Pindos nappe on the top. Each of these nappes consists of a competent series of Mesozoic carbonates, 2–3 km thick, and a thin incompetent cover of flysch, with a maximum thickness of about 1.5 km. After Middle Miocene nappe movements, the whole area became involved in a general uplift and extension (Kowalczyk *et al.* 1977). At the same time the orogenic front migrated westward, and today it reaches the Ionian islands (Doutsos *et al.* 1987).

During this extension, three asymmetric grabens were formed: the Corinth, Rio and Patras grabens (Fig. 2b). The asymmetry of the grabens is largely induced by N-dipping master faults which trend parallel to the coastline of the north Peloponnesus. These grabens form a 140 km long and 40 km wide rift belt, which separates the pre-Neogene folded basement of continental Greece and Peloponnesus. Cumulative vertical displacements along these extensional faults have caused a structural relief with a maximum of 4 km in the Gulf of Corinth and 3 km in the Patras Gulf. Synrift sediments on land attain a maximum thickness of about 1200 m.

Extension has occurred in an area that is still uplifting. Rifted domains subsided relative to the adjacent areas, but subsidence rates rarely exceed uplift rates. Thus, in the northern part of the graben, where the subsidence rates are high, thick lacustrine and marine sediments accumulated. Open marine conditions lasted from the Upper Pliocene until today. This part of the graben is bounded to the south by a major normal fault, which forms a 500 m high submarine escarpment (Jackson *et al.* 1982). Seismic reflection profiles reveal that this fault zone has a listric geometry (Brooks & Ferentinos 1984), accompanied by antithetic tilting of the layers in the down-thrown block. In the middle part, where uplift rates slightly exceed subsidence rates, lacustrine–

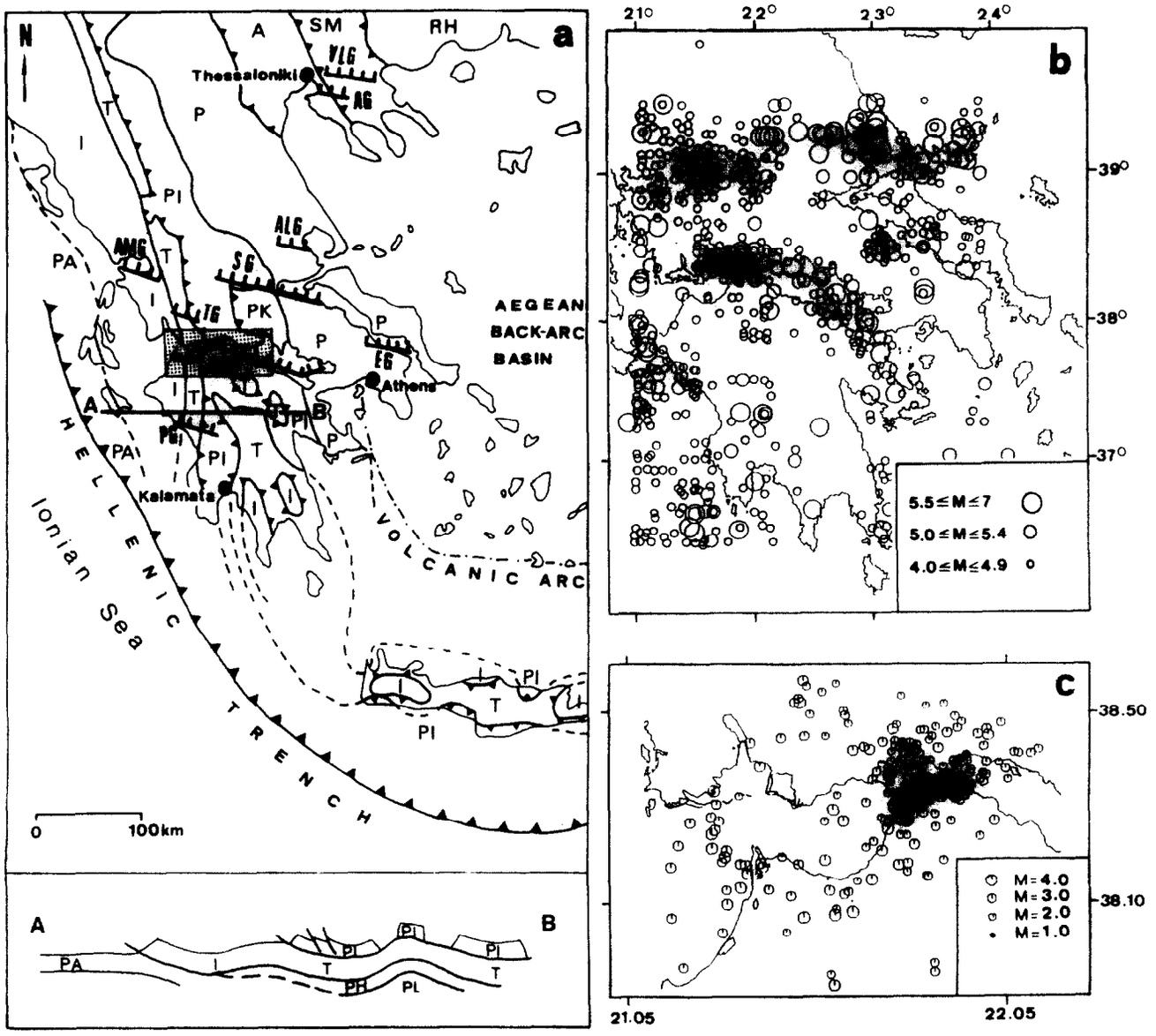

Fig. 1.(a) Post-Miocene, WNW-trending rift-belts transversely cross-cutting the tectonic zones in the Hellenic peninsula. A–B, Schematic section across the Peloponnesus (after Jacobshagen *et al.* 1978). Dotted box: study area. Rift belts: VLG, Volvi–Langada graben; AG, Anthemounta graben; AL.G, Almyros graben; SG, Sperhios graben; AMG, Ambrakia graben; TG, Trihonis graben; EG, Evoikos graben; CPG, Corinth–Patras graben; PG, Pirgos graben. Isopic zones (after Aubouin 1959): RH, Rodopian zone; SM, Serbomacedonian zone; A, Axios zone; P, Pelagonian zone; PK, Parnassos Giona zone; PI, Pindos zone; T, Tripolis zone; PA, Paxos zone; PH, Phyllitic series, Plattenkalk series. (b) Seismicity map of southwestern Greece showing earthquake epicentres ($M > 4$) for the period 1911–1979 (after Papazachos *et al.* 1981). (c) Distribution of microearthquake recorded by PATNET with ML magnitudes in the period June–December 1983 (Melis *et al.* 1989).

brackish marls were covered by shallow marine marls, fluvial deposits and marine terraces (Figs. 2a and 3a & b). As revealed by chronostratigraphical studies (Symeonidis *et al.* 1987, Frydas 1988, 1989), these marls were deposited from Upper Pliocene to Lower Pleistocene. In the southern part of the graben, uplift dominates, whereas differential subsidence never reached sea level (Fig. 3c). In the rifted margins, where low subsidence rates occur, alluvial fans were deposited. As a result of basinward increasing subsidence, Gilbert-type fan deltas were accumulated above marls (Fig. 3c).

On the basis of the stratigraphy given in Fig. 2(a) the following evolutionary picture can be proposed. Subsidence began in the Upper Pliocene at the northern part of the grabens (Fig. 3a) and lasted until the present. In Quaternary time, by further continuation of rifting, subsidence and extension migrated southward with time, by progressive outward stepping of fault activity. Moreover, the coastal areas of the grabens have been affected by large-scale faulting events and a thick sequence of alluvial fan delta and alluvial fan deposits accumulated across them (Figs. 3b & c).

In addition, subsidence migrates from east to west along the rift axis (Fig. 3, A′–B′ and C–D). In the Upper Pliocene, the Patras Gulf and East Corinth Gulf were formed (Fig. 3). In the Quaternary, rifting propagated westward, along the Corinth graben axis, until it reached the Rio graben. This graben is reactivated as a major transfer zone along which extension shifted southwestwards to form the Patras graben.

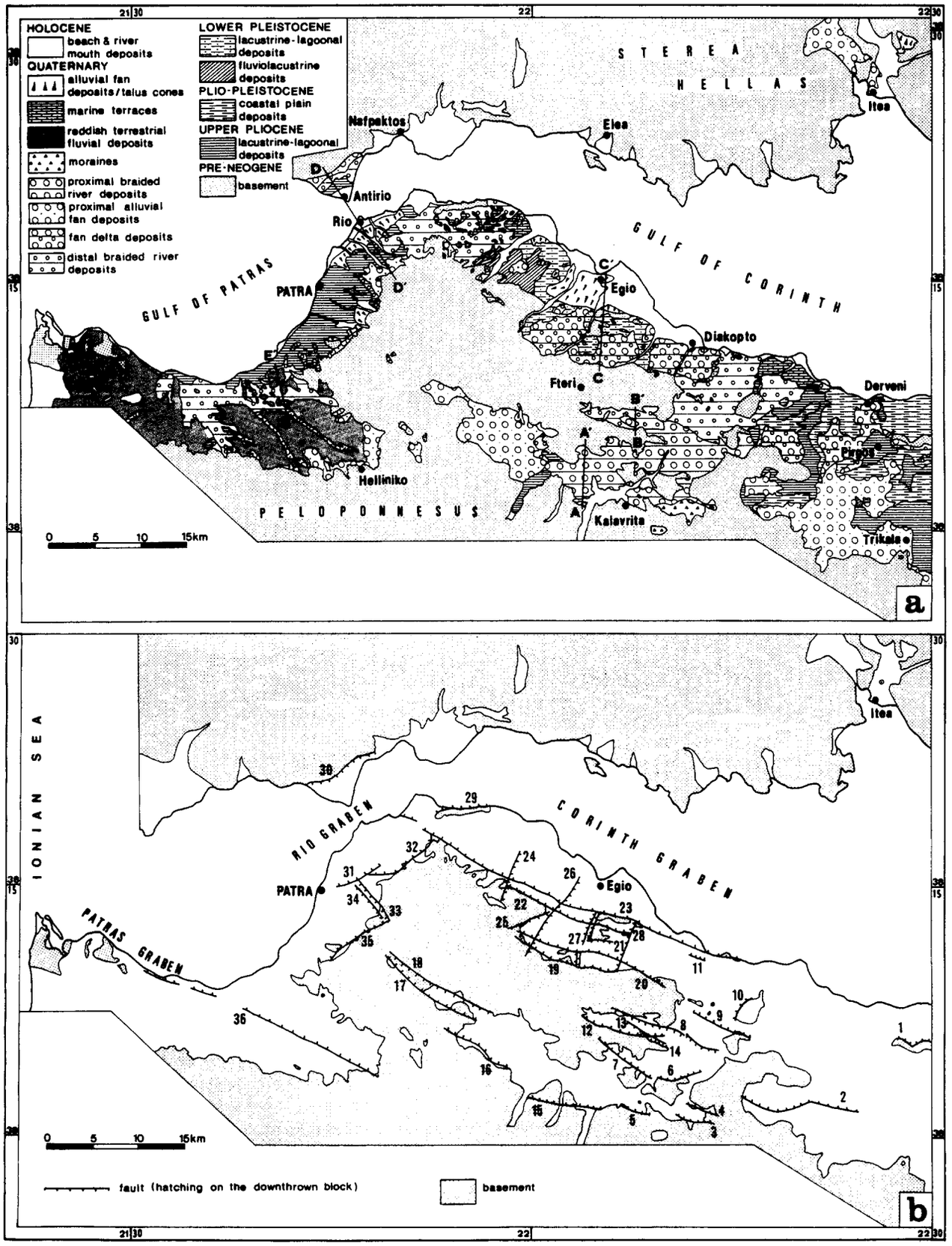

Fig. 2.(a) Geological map of the western part of the Corinth–Patras rift. (b) Tectonic map showing the major active faults with known displacement at the Earth's surface.

GEOMETRY OF ACTIVE FAULTS

We have described as active all faults which displace Quaternary deposits or cross-cut the present topography. About 500 active faults with length greater than 1.5 km have been mapped in NW Peloponnesus.

Most of the WNW-trending normal faults show a curved listric geometry in mesoscopic scale (Doutsos &

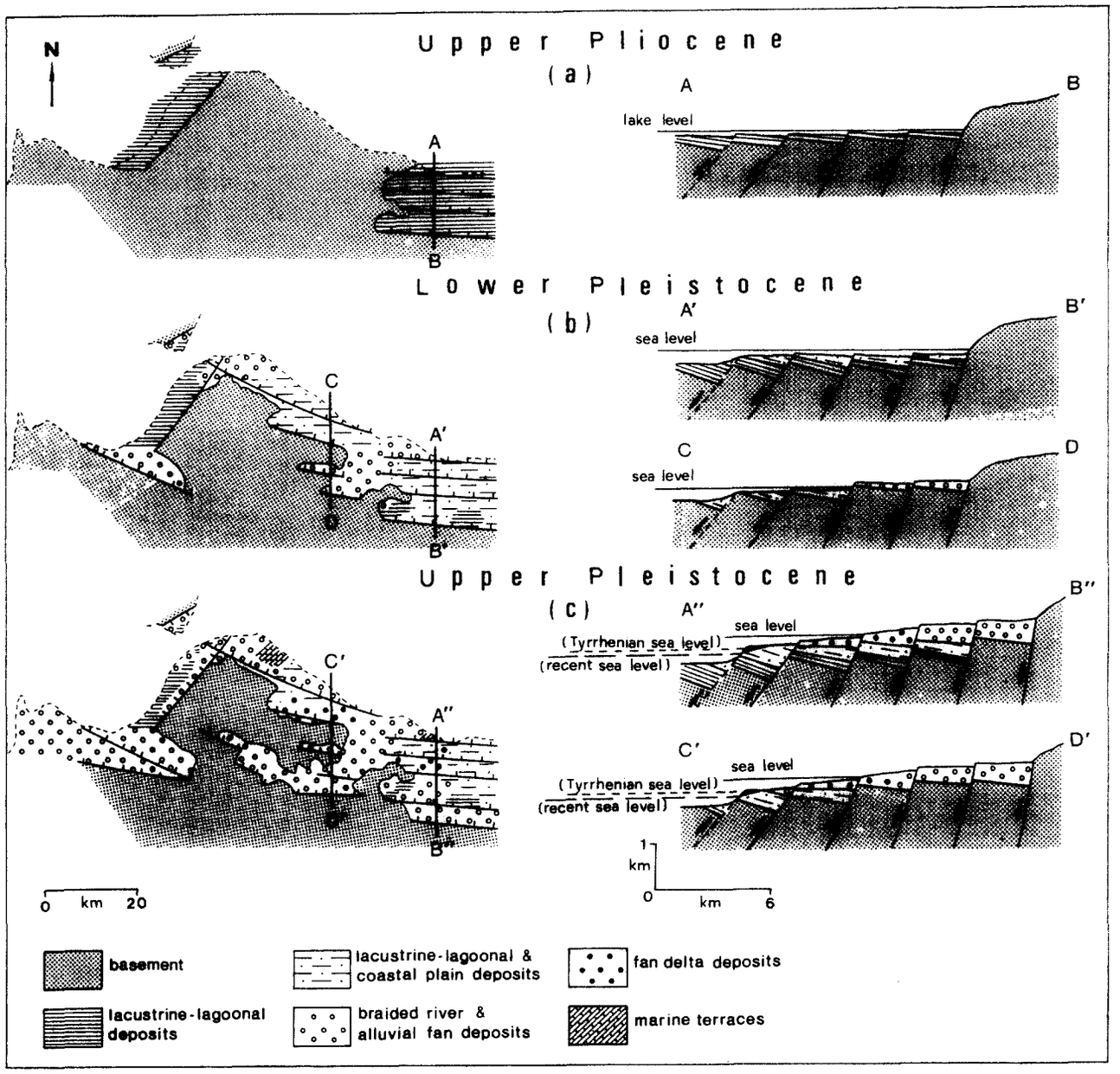

Fig. 3. Maps and cross-sections showing the paleogeographic evolution of the western part of Corinth–Patras rift in three stages (a, b and c).

Piper 1990). A similar geometry of fault plane has also been observed at map scale. Major faults cross-cutting vertical cliffs show a down-dip decrease of their dips. Each of these major listric faults is accompanied by between one and four synthetic faults (Fig. 4, C–C'), one or more counter faults and a roll-over anticline with highly rotated layering (Fig. 4, A–A' and C–C'). These faults divide the cross-sections A–A', B–B' and C–C' into a series of blocks, wider to the south than to the north. Fault dips at the Earth's surface range between 50° and 80°. Many of these major normal faults in the eastern Corinth graben are seismically active and show a listric geometry.

The major master faults have produced large N-dipping fault scarps, whereas all other accommodation fractures produce fault scarplets and flexure scarps. Scarp heights commonly reach 300 m. Scarps are often well preserved in conglomeratic rocks (fault 11 in Fig. 2b), whereas extensive erosion accompanied by landslides in fine-grained conglomerates produces slope retreat (faults north of Antirio in Fig. 4, D–D') and shallower morphological depressions. Large, wedge-shaped sedimentary prisms were formed by repeated reactivation of the faults scarps (Fig. 4, A–A', D–D') throughout the Quaternary. Thus, faults cross-cutting folded basement seem to have been active during the Quaternary sedimentation. In many cases active faults continue uninterrupted from the folded basement into the overlying Quaternary sediments (Fig. 4, C–C', D–D').

The number of active faults varies from region to region (Fig. 2b). In regions with a high density, e.g. south of Egio, faults are longer in length and more intense in seismic activity. However, fault traces rarely exceed 10 km. Even large normal faults, such as the Eliki fault, south of Egio, or the Pyros fault, in the Patras

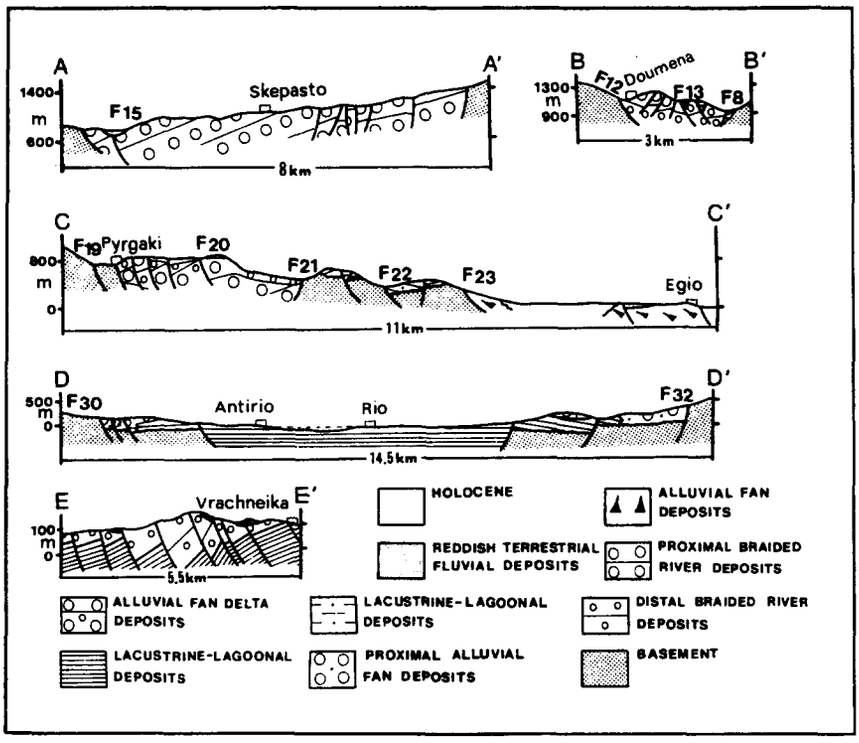

Fig. 4. Geological cross-sections in the western part of Corinth–Patras rift. The locations of the cross-sections are shown in Fig. 2(a).

graben (faults 23 and 36 in Fig. 2b), are rarely continuous at the surface along strike for more than 10 km. They are clearly segmented along strike. In most cases the normal faults die out along their lengths showing different displacement along strike. In other cases normal faults (Fig. 2b, fault 22) terminate against transfer faults (Fig. 2b, faults 24 and 28). In the central Corinth graben sedimentary processes are strongly influenced by NNE-trending, steeply-dipping transfer faults (Fig. 2b) (Poulimenos *et al.* 1989). These faults separate emerging narrow barriers from intervening broad valleys, like that extending between Kalavrita and the Gulf area (Fig. 2a). Sedimentary features on the barriers are very coarse, whereas, in the valleys, finer material is deposited.

KINEMATICS OF FAULTS

As indicated by slickensides, the kinematic picture is characterized by dip-slip movement along WNW-trending normal faults (Fig. 5a). Two other sets of faults, one pre-existing ENE-trending fault set (Figs. 5b & a) and a new NNE-trending fault set (Fig. 5c), show both normal and strike slip motions and act as transfer faults.

The total geologic offset across the neotectonic faults near the Earth's surface can be estimated by adding the maximum thickness of the sedimentary prism, which is deposited in the hangingwall block of the fault, and the height of the fault scarp. However, this estimate will be inaccurate if there has been a large amount of erosion either beneath or above the hanging-wall sediments. Table 1 gives total offset estimations for 36 major active faults in the study area (Fig. 2b). To estimate other characteristics of these major faults at depth, a displacement analysis of the faults has been carried out. Many recent papers (i.e. Muraoka & Kamata 1983, Williams & Chapman 1983, Pfiffner 1985, Barnett *et al.* 1987, Walsh & Watterson 1988) show that displacement on a fault surface varies from a maximum point to zero at their edges.

The following terminology has been used in this paper (Fig. 6):

h, maximum dimension of the fault surface in the direction parallel to the slip direction (referred as the down-dip width of the fault) (Sibson 1989);

l, maximum length of the fault on the Earth's surface;

d, dip separation at the Earth's surface of a normal fault;

d_{max}, maximum dip separation of a normal fault.

The measurements of h, d and d_{max} in 170 mesoscopic faults have been obtained from the surfaces of vertical cliffs up to 250 m height (Fig. 7). As mesoscopic faults and major faults have a similar geometry, their displacement analysis can be used to determine characteristics of major faults at depth.

To estimate the relationship between the fault displacement at the Earth's surface (d) and the maximum displacement at depth (d_{max}), 20 fully exposed mesoscopic faults were measured (Fig. 7a). The linear trend of the data on a log–log plot gives rise to the expression:

$$\log d_{max} = a \log d + b.$$

By using the method of least-squares regression the

Table 1. Behavior data for 36 seismogenic faults shown in Fig. 2(b).

No. of faults	Length l (m)	Fault displacement at the Earth's surface d (m)	Maximum fault displacement d_{max} (m)	Width h (m)	Stratigraphic age	Assumed age t (Ka)	Slip-rate s (mm year^{-1})	Rupture area A (m^2)	Magnitude M	Magnitude M^*	Coseismic average slip u ($\times 10^{-1}$)	Recurrence interval R
1	9000	800	950	13,800	Base of Upper Pliocene sediments	3200	0.29	1.24×10^8	6.0	6.24	4.0	1380
2	13,000	700	850	12,400	Base of Upper Pliocene sediments	3200	0.26	1.61×10^8	6.2	6.35	4.4	1690
3	5500	70	125	2000	Since deposition of moraine	100	1.25	1.10×10^7	5.0		1.0	80
4	4000	160	250	3900	Since deposition of fluvial strata on hangingwall	700	0.35	1.56×10^7	5.2		1.4	400
5	3600	240	350	5350	Since deposition of fluvial strata on hangingwall	700	0.50	1.92×10^7	5.3		1.5	300
6	4800	500	650	9600	Base of Quaternary sediments	1800	0.36	4.60×10^7	5.6	5.81	2.2	610
7	7200	500	650	9600	Base of Quaternary sediments	1800	0.36	6.91×10^7	5.8	5.98	2.7	750
8	13,000	250	360	5500	Base of Quaternary sediments	1800	0.51	7.15×10^7	5.8	6.00	2.7	530
9	8000	500	650	9600	Base of Quaternary sediments	1800	0.36	7.68×10^7	5.8	6.03	2.7	750
10	2800	500	650	9600	Base of Quaternary sediments	1800	0.36	2.68×10^7	5.4		1.7	470
11	2000	300	420	6350	Since deposition of fan delta	700	0.60	1.27×10^7	5.1		1.2	200
12	9000	150–500	240–650	3700–9600	Base of Quaternary sediments	1800	0.13–0.36	5.98×10^7†	5.8	5.92	2.7	750
13	5000	100	170	2700	Since deposition of proximal braided river deposits on hangingwall	700	0.24	1.35×10^7	5.1		1.2	500
14	2800	200	300	4600	Base of Quaternary deposits	1800	0.16	1.28×10^7	5.1		1.2	750
15	8600	450	590	8700	Since deposition of fluvial strata on hangingwall	700	0.84	7.48×10^7	5.8	6.02	2.7	320
16	10,000	350	480	7200	Since deposition of alluvial fans on hangingwall	700	0.68	7.20×10^7	5.8	6.00	2.7	400
17	13,000	200	300	4600	Since deposition of alluvial fans on hangingwall	700	0.42	5.98×10^7	5.7	5.92	2.4	570
18	11,000	200	300	4600	Since deposition of alluvial fans on hangingwall	700	0.42	5.06×10^7	5.7	5.85	2.4	570
19	12,000	200–800	300–950	4600–13,800	Main fault activity since deposition of fan delta on hangingwall	700	0.16–0.76	1.10×10^8†	6.0	6.19	4.0	525
20	18,000	200–700	300–850	4600–12,400	Base of Quaternary sediments	1800	0.16–0.47	1.55×10^8†	6.1	6.34	4.0	850
21	2400	300	420	6350	Base of Quaternary sediments	1800	0.23	1.52×10^7	5.1		1.2	520
22	15,000	200–500	300–650	4600–9600	Base of Quaternary sediments	1800	0.16–0.36	1.06×10^8†	6.0	6.17	4.0	1110
23	40,000	800	950	13,800	Base of Quaternary sediments	1800	0.52	5.52×10^8	6.7	6.89	8.0	1540
24	6000	150	240	3700	Base of Quaternary sediments	1800	0.13	2.22×10^7	5.3		1.5	1150
25	3500	150	240	3700	After deposition of lacustrine–lagoonal strata on hangingwall	700	0.34	1.29×10^7	5.1		1.2	350
26	11000	100	170	2700	Since deposition of alluvial fans on hangingwall	700	0.24	2.97×10^7	5.5	5.62	1.9	790
27	6000	450	590	6800	Base of Quaternary sediments	1800	0.32	4.08×10^7	5.6	5.76	2.2	650
28	5500	250	360	5500	Base of Quaternary sediments	1800	0.20	3.02×10^7	5.5	5.63	2.0	1000
29	6000	>150	>240	>3700	Base of Quaternary sediments	1800	>0.13	$>2.20 \times 10^7$	>5.3		>1.5	—
30	8600	350	480	7200	Since deposition of alluvial fans on hangingwall	700	0.68	6.19×10^7	5.8	5.94	2.7	400
31	5700	80	140	2250	Fault activity identified since deposition of alluvial fans	700	0.20	1.28×10^7	5.0		1.0	500
32	9500	800	950	13,800	Since deposition of alluvial fans on hangingwall	700	1.35	1.31×10^8	6.1	6.26	4.0	300
33	6000	200	300	4650	Fault activity identified since deposition of fluvial strata	1800	0.16	2.79×10^7	5.4		1.7	1060
34	4500	150	240	3700	Fault activity identified since deposition of fluvial strata	1800	0.13	1.66×10^7	5.2		1.4	1080
35	8000	250	360	5500	Fault activity identified since deposition of alluvial fans	700	0.51	4.40×10^7	5.6	5.79	2.2	430
36	28,300	500	650	9600	Base of Quaternary sediments	1800	0.36	2.71×10^8	6.4	6.58	5.5	1530

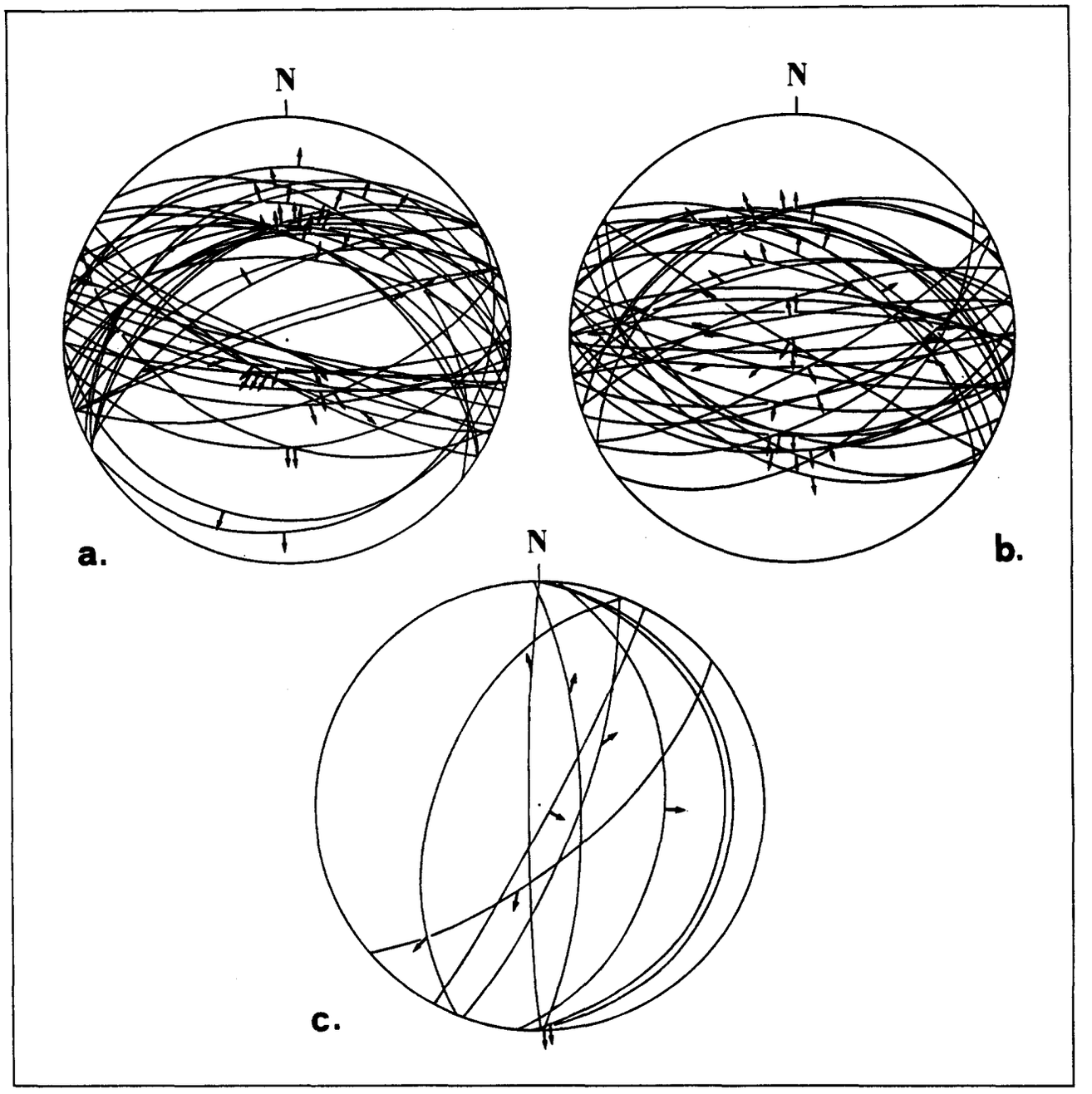

Fig. 5. Stereographic projections of faults and slickensides (arrows) on mesoscopic faults, from Corinth graben (a and c) and Rio–Patras graben (b).

best-fit line through the most d, d_{max} data ($R^2 = 92\%$), can be expressed as:

$$\log d_{max} = 0.83 \log d + 0.57, \quad (1)$$

with standard deviation of $\log d_{max} = \pm 0.14$.

For estimating the d_{max}–h relation, data of 150 mesoscopic faults have been collected in synrift sediments (silts–sands and conglomerates) and in the folded basement (Fig. 7b). The data define a linear band on a log–log plot corresponding to variation in maximum fault displacement of approximately one order of magnitude for a given fault width. The best-fit line through most h–d_{max} data ($R^2 = 73\%$), obtained by least-squares regression, can be expressed as:

$$\log h = 0.95 \log d_{max} + 1.31 \quad (2)$$

with standard deviation of $\log h = \pm 0.12$.

Combining equations (1) and (2), the down-dip width (h) of 36 faults with known displacement at the Earth's surface has been estimated in Table 1.

Average slip rates (s) have been obtained from

Notes to Table 1:

l and d are obtained from field observations.
d_{max} and h are estimated from equations (1) and (2).
Stratigraphic age is based on biostratigraphic studies.
$s = d_{max}/t$.
$A = l \cdot h$; †the measured rupture area is obtained by $A = (h_{min}+h_{max}) \times 1/2$.
M values are based on tables from Sibson (1989), M^* values are estimated from $M = \log A + 4.15$, $M > 5.6$ with A in km^2 (Wyss 1979).
u is based on tables from of Sibson (1989).
$R = u/s$.

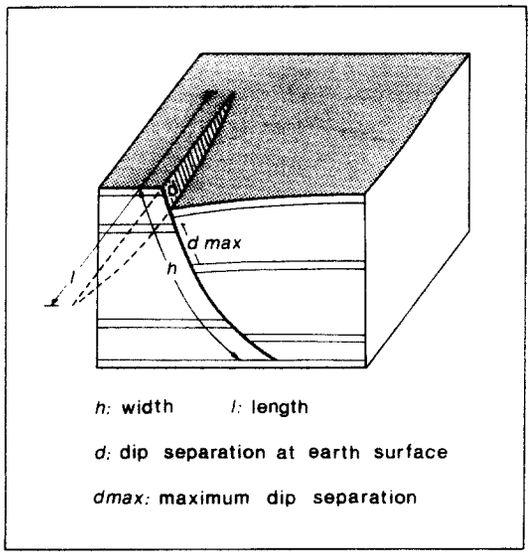

Fig. 6. Block diagram illustrating schematically fault dimensions l, h and d–d_{max} relation.

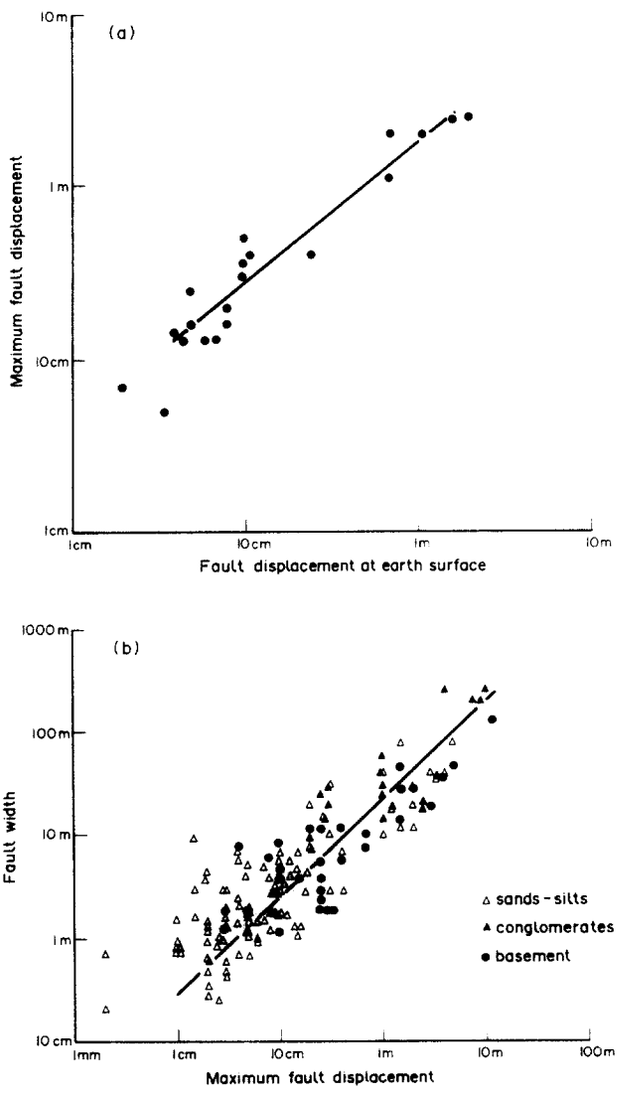

Fig. 7.(a) Logarithmic plot of maximum fault displacement against fault displacement at the Earth's surface for 20 faults. (b) Logarithmic plot of down-dip fault width against maximum fault displacement for 150 faults.

amounts of the total geologic offset divided by the age of the fault (Table 1). The age of 36 faults was estimated to be from 3.2 to 0.09 Ma, based on biostratigraphic work in the top series of the basal rift sequence which reveals lower Pleistocene age (Symeonidis *et al.* 1987, Frydas 1989, Mountzos 1990).

SEISMOTECTONICS

Earthquake epicentres in central Greece define a 200 km long and 40 km wide belt across the Hellenides from the Aegean to the Ionian Sea (Fig. 1b). The central part of this belt is occupied by the Corinth–Patras rift. The northern submerged part of the rift is much more tectonically active than the southern margin in north Peloponnesus. An intense spatial clustering of seismicity is recorded between Rio and Nafpaktos (Drakopoulos *et al.* 1987, Melis *et al.* 1989) (Fig. 1c), in a tectonically unstable area caused by the intersection of the Rio and Corinth grabens (Doutsos *et al.* 1985).

Sharp changes in the number of epicentres occur west of the Rio–Antirio strait (Fig. 1c), with very low numbers in the Patras Gulf. Since the Patras Gulf is a major asymmetric graben of late Quaternary origin (Ferentinos *et al.* 1985), a dominantly aseismic deformation for this area may be occurring. This aseismic deformation may be attributed to salt deposits underlying the Patras Gulf (Ferentinos *et al.* 1985, Brooks *et al.* 1988). The salt deposits may have decoupled the sedimentary cover from the folded basement, thus inhibiting fault propagation from the basement upwards, as described in the Hellenic trench (Jackson & McKenzie 1988). Seismic activity in the Corinth and Patras grabens is largely restricted to the upper one third of the continental crust (<15 km, Tselentis & Makropoulos 1986), as in other extended continental terranes (Das & Scholz 1981, Sibson 1982).

A prediction for the maximum expected earthquake magnitude (M_{max}) along each of the 36 active faults was attempted, under the assumption that the entire fault will rupture in one event. For this purpose the maximum rupture area (A) of each of the 36 active faults was calculated from $A = l \cdot h$ (where l is taken from the length of the fault in Fig. 2b). This estimate will be inaccurate if the surface rupture lengths (l) are essentially smaller than the source lengths, which occur deeper in the crust. Also uncertainties arise from the field calculations of d (see previous section).

The maximum magnitude of the expected earthquakes is calculated from A, on the basis of relationships discussed by Wyss (1979, equation 5) and Sibson (1989, table 1) (see Table 1). These relations obtained from worldwide data, are valid in the Corinth–Patras rift, because the average energy density in the Earth's crust is approximately constant, as evidenced by the constancy of stress drop associated with large crustal earthquakes. By using the equation of Wyss (1979), the expected maximum magnitudes, M, have been overestimated by ~20%. This variability of M estimates is probably due to

different methods used by these authors to estimate the rupture area.

The maximum magnitude (M) of the expected earthquakes along the major seismogenic faults in the studied area (Table 1) ranges between 5.0 and 6.7. Only eight faults are capable of generating earthquakes larger than $M = 6$. However, it must be pointed out that an earthquake with a magnitude $M = 5$, such as the one that occurred in Patras city on 15 May 1989, was associated with surface rupture of 2.5 km and maximum coseismic displacement of 10 cm. Thus, we conclude that the minimum known magnitude of a surface-rupturing earthquake is $M = 5$.

Some difficulties in the prediction for the maximum expected earthquake magnitude arise in the cases where seismogenic faults (faults 12, 19, 20 and 22 in Table 1) exhibit marked changes in the amount of vertical throw along strike. In such cases, fault width ranges from a maximum (h_{max}) to a minimum value (h_{min}) (as derived from equations 1 and 2), and A can be estimated from $A = (h_{min}+h_{max}) \times l/2$.

Seismic studies in the east Corinth graben (King *et al.* 1985) and in the Kalamata area (Fig. 1a) (Lyon *et al.* 1988) reveal that seismogenic faults capable of producing large earthquakes dip at angles of 40–50° and extend downwards to the base of the seismogenic layer at a depth of 8–12 km. This confirms our estimations that the major faults of the Corinth graben, with maximum displacement of about 1000 m, have a down-dip width of around 14 km and extend to a depth of 10 km (Fig. 8). However, if the uncertainties of equations (1) and (2) are compounded, this depth estimate will range between 7.4 and 13 km, whereas M estimates will vary ±10% in Table 1.

Assuming that the same slip distribution associated with the maximum earthquake magnitude is repeated at any point along the fault in successive events (Wesnousky *et al.* 1983, Schwartz & Coppersmith 1984), and that the fault slip is all released seismically, the recurrence time of earthquakes can be obtained from the equation $R = u/s$ (Yeats 1988), where R is the recurrence time (years), u is the coseismic average slip and s is the slip rate of the fault. For each of the 36 faults s is known (Table 1), whereas u can be estimated from Sibson (1989). Thus, we estimate that the recurrence time intervals in the study area varies between 80 and 1690 years.

TECTONIC SYNTHESIS

In order to describe upper crustal deformation in the western Corinth graben, the cross-section (Fig. 8) passing through Elea, Egio and Kalavrita (for locations see Fig. 2a) was chosen. From north to south three domains of different structural evolution can be distinguished:

(1) a major listric fault which has been active since Lower Pleistocene marks the southern edge of a deep asymmetric graben filled by the sea. Displacement along this fault is in excess of 1000 m. Most of the seismic epicentres are clustered along this fault;

(2) a 10 km wide zone, in the middle, with two major asymmetric grabens. The sedimentary infilling of these grabens show a progressive evolution from open marine conditions in the Lower Pleistocene, to terrestrial conditions in the Upper Pleistocene. The graben forming faults reach a depth of about 10 km and show maximum displacements between 240 and 950 m. This area is characterized by an intermediate seismic activity and earthquakes with maximum magnitude of between 5.1 and 6.7;

(3) a 15 km wide zone, in the south, with three

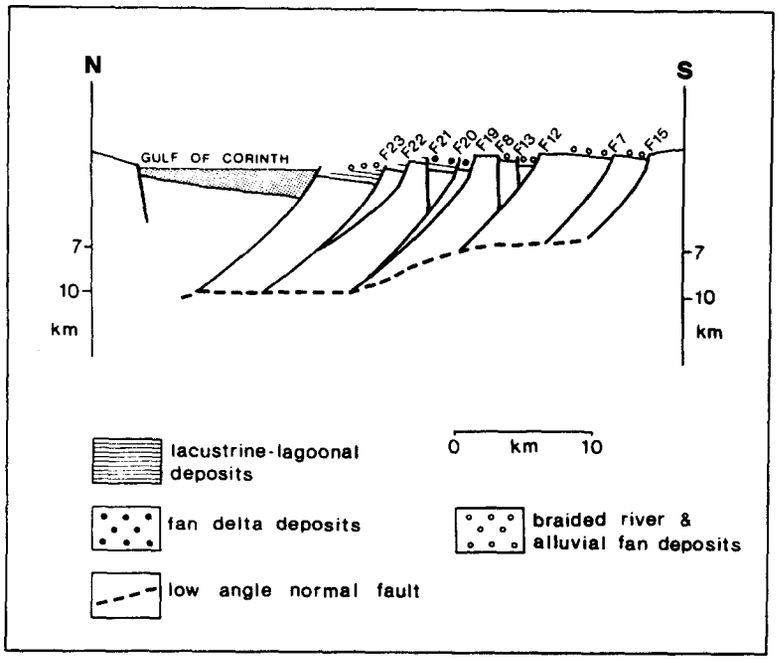

Fig. 8. Schematic section across the Corinth graben between Kalavrita, Egio and Elea (Fig. 2a). The width and displacement estimates of the faults are derived from Table 1.

asymmetrical grabens which are filled by terrestrial deposits. These grabens are bounded to the south by faults which reach a depth of about 7 km and show maximum displacements of between 240 and 650 m. This area is characterized by low seismic activity and earthquakes with maximum magnitudes of between 5.0 and 5.8.

This synoptic presentation of structural data led us to assume the presence of a large curved ramp in the upper crust, as has been described from many continental rifts in the world (e.g. Bosworth 1985, Gibbs 1987). Localized continuing deep-seated extension under the Corinth Gulf area is synchronous with the process of diminished faulting and uplift in the southern rift margin. This tectonic picture may be caused by the subsequent curving and uplift of a low-angle detachment fault, as proposed by Morley (1989) and Perry & Schamel (1990).

The structural asymmetry illustrated in Fig. 8 is representative of most of the WNW-trending rift zones of the Hellenic Arc (Doutsos & Piper 1990) and seems to preclude the pure shear model. Low extension, about 5 km lengthening of a 25 km long cross-section (Fig. 8), and the progressive widening of the rifts favour a slow extensional model in which the décollement horizon lies at a mid-crustal level (Kusznir & Park 1987). The nature of the basal stress required to explain the structural asymmetry will be the subject of future geodynamic research.

Acknowledgements—This work has been supported by the Greek Organization for Earthquake Protection, Athens, and by the Volkswagen Stiftung, Hannover. We thank Drs A. Tselentis and G. Papatheodorou for their valuable suggestions in computing. The paper has also benefitted greatly from the comments of the reviewers, Dr C. M. de Polo and Professor D. J. Sanderson.

REFERENCES

Angelier, J. 1979. Neotectonique de l'arc Egeen. *Spec. Publ. Soc. Geol. N.* **3**, 418.

Aubouin, J. 1959. Contribution a l'etude geologique de la Greece septentrionale: les confins de l'Epire et de la Thessalie. *Annls Geol. Pays Hellen.* **10**.

Barnett, J., Mortimer, J. Rippon, J. Walsh, J. & Watterson J. 1987. Displacement geometry in the volume containing a single normal fault. *Bull. Am. Ass. Petrol. Geol.* **71**, 925–937.

Bosworth, W. 1985. Geometry of propagating continental rifts. *Nature* **316**, 625–627.

Brooks, M., Clews, J. E., Melis, N. S. & Underhill, J. 1988. Structural development of Neogene basins in western Greece. *Basin Res.* 1, 129–138.

Brooks, M. & Ferentinos, G. 1984. Tectonics and sedimentation in the Gulf of Corinth and the Zakynthos and Kefallinia Channels, western Greece. *Tectonophysics* **101**, 25–54.

Das, S. & Scholz, C. H. 1981. Off-fault aftershock clusters caused by shear stress increase. *Bull. seism. Soc. Am.* **71**, 1669–1675.

Dercourt, J. 1964. Contribution a Peloponnese septentrional. *Annls Geol. Pays Hellen.* **15**.

Dewey, J. F. & Şengör, A. M. C. 1979. Aegean and surrounding regions: complex multiplate and continium tectonics in a convergent zone. *Bull. geol. Soc. Am.* **90**, 84–92.

Doutsos, T. 1980. Postalpine Geodymamic Thessaliens (Griechenland). *Z. dt. geol. Ges.* **131**, 685–698.

Doutsos, T., Kontopoulos, N. & Ferentinos, G. 1985. Das westliche Ende des Korinth-Grabens. *Neues Jb. Geol. Paläont. Mh.* **11**, 652–666.

Doutsos, T., Kontopoulos, N. & Frydas, D. 1987. Neotectonic evolution of northwestern continental Greece. *Geol. Rdsch.* **76**, 433–450.

Doutsos, T., Kontopoulos, N. & Poulimenos, G. 1988. The Corinth-Patras rift as the initial stage of continental fragmentation behind an active island arc (Greece). *Basin Res.* **1**, 177–190.

Doutsos, T. & Piper, D. 1990. Listric faulting, sedimentation and morphological evolution of the Quaternary eastern Corinth rift, Greece: First stages of continental rifting. *Bull. geol. Soc. Am.* **102**, 812–829.

Drakopoulos, I., Makropoulos, I. Latousakis, I. Stayrakakis, G. & Tselentis, A. 1987. *Seismologic Studies in the Rio–Antirio Area.* University of Athens.

Ferentinos, G., Brooks, M. & Doutsos, T. 1985. Quaternary tectonics in the Gulf of Patras, Western Greece. *J. Struct. Geol.* **7**, 713–717.

Frydas, D. 1988. Kalkiges Nannoplankton aus dem Neogen von NW-Peloponnes. *Neues Jb. Geol. Paläont. Mh.* **5**, 275–286.

Frydas, D. 1989. Biostratigraphische Untersuchungen aus dem Neogen der NW- und W-Peloponnes, Griechenland. *Neues Jb. Geol. Paläon. Mh.* **6**, 321–344.

Gibbs, A. P. 1987. Development of extension and mixed-mode sedimentary basins. In: *Continental Extensional Tectonics* (edited by Coward, M. P., Dewey, J. F. & Hancock, P. L.). *Spec. Publs geol. Soc. Lond.* **28**, 19–33.

Jackson, J., Gagnepain, J., Houseman, G., King, G. C. P., Papadimitriou, P., Soufleris, C. & Virieux, J. 1982. Seismicity, normal faulting and the geomorphological development of the Gulf of Corinth (Greece): The Corinth earthquakes of February and March 1981. *Earth Planet. Sci. Lett.* **57**, 377–397.

Jackson, J. & McKenzie, D. 1988. The relationship between plate motions and seismic moment tensors and the rates of active deformation in the Mediterranean and Middle East. *J. Geophys.* **93**, 45–73.

Jacobshagen, V., Durr, S., Kockel, F., Kopp, K. O. & Kowalczyck, G. 1978. Structure and geodynamic evolution of the Aegean region. In: *Alps, Apennines, Hellenides* (edited by Closs, H. *et al.*). *Scient. Rep.* **38**, 455–477.

King, G. C. P., Ouang, Z. X., Papadimitriou, P., Deschamps, A., Gagnepain, J., Houseman, G., Jackson, J. A., Soufleris, C. & Virieux, 1985. The evolution of the Gulf of Corinth (Greece): an aftershock study of the 1981 earthquakes. *Geophys. J. R. astr. Soc.* **80**, 677–693.

Kontopoulos, N. & Doutsos, T. 1985. Sedimentology and tectonics of the Antirion area (Western Greece). *Bull. Soc. geol. It.* **104**, 479–489.

Kowalczyk, V., Richter, D., Risch, H. & Winter, K. P. 1977. Zur zeitlichen Einstufung der tektogenetischen Ereignisen auf dem Peloponnes. *Neues Jb. Geol. Paläont. Mh.* **9**, 549–564.

Kusznir, N. J. & Park, R. G. 1987. The extensional strength of the continental lithosphere and thickness. In: *Continental Extensional Tectonics* (edited by Coward, M. P., Dewey, J. F. & Hancock, P. L.). *Spec. Publs geol. Soc. Lond.* **28**, 35–52.

Lyon, H., Caen, H., Armijo, R., Drakopoulos, J., Baskoutas, J., Delibasis, N., Gaulon, R., Kouskouna, V., Latoussakis, J., Makropoulos, M., Papadimitriou, P., Papanastasiou, D. & Pedotti, G. 1988. The 1986 Kalamata (South Peloponnesus) earthquake: detailed study of a normal fault, evidence for east–west extension in the Hellenic Arc. *J. geophys. Res.* **93**, 14,967–15,000.

McKenzie, D. P. 1978. Active tectonics of the Alpine–Himalayan belt: the Aegean Sea and surrounding regions. *Geophys. J. R. astr. Soc.* **55**, 217–254.

Melis, N., Brooks, M. & Pearce, R. 1989. Microearthquake study in the Gulf of Patras region, western Greece, and its seismotectonic interpretation. *J. geophys. Res.* **98**, 515–524.

Mercier, J. L. 1977. Principal results of a neotectonic study of the Aegean Arc and its localisation within the eastern Mediterranean. *Proc. 6th Colloquim on the Geology of the Aegean Region, Athens* **3**, 1281–1291.

Morley, C. K. 1989. Extension, detachments and sedimentation in continental rifts (with particular reference to the East Africa). *Tectonics* **8**, 1175–1192.

Mountzos, T. 1990. Palynologische Untersuchungen zur Palaoklimatologie und stratigraphie der postorogen sedimente des NW-Peloponnes. Unpublished Thesis, University of Munster.

Muraoka, D. & Kamata, H. 1983. Displacement distribution along minor fault traces. *J. Struct. Geol.* **5**, 483–495.

Papazachos, B. C., Mountrakis, D., Psilovikos, A. Leventakis, G. 1979. Surface fault traces and fault-plane solutions of the May–June 1978 shocks in the Thessaloniki area, Greece. *Tectonophysics* **53**, 171–183.

Papazachos, B., Comninakis, P., Mountrakis, D. & Pavlides, S. 1981. Preliminary results of an investigation of the February–March Alkionides Gulf (Greece) earthquakes. *Int. Symp. on Hellen. Arc and Trench* **2**, 74–87.

Pavlides, S. & Moundrakis, D. M. 1987. Extensional tectonics of NW Macedonia (Greece) since Miocene. *J. Struct. Geol.* **9**, 385–392.

Perry, S. T. & Schamel, S. 1985. The role of low-angle normal faulting and isostatic response in the evolution of the Suez rift, Egypt. *Tectonophysics* **174**, 159–173.

Pfiffner, A. 1985. Displacement along thrust faults. *Eclog. geol. Helv.* **78**, 313–333.

Philippson, A. 1892. *Der Peloponnes, Versuch eine Landeskunde auf geologische Grundlage*. Friedleander, Berlin.

Poulimenos, G., Albers, G. & Doutsos, T. 1989. Neotectonic evolution of the central section of the Corinth graben. *Z. dt. geol. Ges* **140**, 173–182.

Schwartz, D. P. & Coppersmith, K. J. 1984. Fault behavior and characteristic earthquakes: examples from the Wasatch and San Andreas fault zones. *J. geophys. Res.* **89**, 5681–5698.

Sebrier, M. 1977. Tectonique Recent d'une tranversale a l'Arc Egeen. Unpublished Ph.D. thesis, Universite de Paris-Sud, Centre d'Orsay.

Sibson, R. H. 1982. Fault zone models heat flow and depth distribution of earthquakes in the continental crust of the United States. *Bull. seism. Soc. Am.* **72**, 151–163.

Sibson, R. H. 1989. Earthquake faulting as a structural process. *J. Struct. Geol.* **11**, 1–14.

Symeonidis, N., Theodorou, G., Schutt, H. & Velitzelos, E. 1987. Paleontological and stratigraphic observations in the area of Achaia and Etoloakarnania (W. Greece). *Annls Geol. Pays Hellen.* **38**, 317–353.

Tselentis, G. A. & Makropoulos, K. 1986. Rates of crustal deformation in the Gulf of Corinth (central Greece) as determined from seismicity. *Tectonophysics* **24**, 55–61.

Walsh, J. & Watterson, J. 1988. Analysis of the relationship between displacements and dimensions of faults. *J. Struct. Geol.* **10**, 239–247.

Wesnousky, S. G., Scholz, C. H. Shimazaki, K. & Matsuda, T. 1983. Earthquake frequency distribution and the mechanics of faulting. *J. geophys. Res.* **88**, 9331–9340.

Williams, G. & Chapman, T. 1983. Strain development in the hanging-walls of thrusts due to their slip/propagation rate: a dislocation model. *J. Struct. Geol.* **5**, 563–571.

Wyss, M. 1979. Estimating maximum expectable magnitude of earthquakes from fault dimensions. *Geology* **7**, 336–340.

Yeats, R. 1988. Late Quaternary slip rate on the Oak Ridge fault, tranverse ranges, California: Implications for seismic risk. *J. geophys. Res.* **93**, 12,137–12,149.

Zelilidis, A., Koukouvelas, J. & Doutsos, T. 1988. Neogene paleostress changes behind the forearc fold belt in the Patraikos Gulf area, western Greece. *Neues Jb. Paläont. Mh.* **5**, 311–325.